Chloric Acid-Driven Nucleation Enhanced by
Dimethylamine and Sulfuric acid in the Arctic:
Mechanistic Study
Shengming Wang ² , Huidi Zhang ¹ , Xiangli Shi ^{1,*} , Qingzhu Zhang ² ,
Wenxing Wang ² , Qiao Wang ²
¹ College of Geography and Environment, Shandong Normal
University, Jinan 250014, P. R. China
² Environment Research Institute, Shandong University,
Qingdao 266237, P. R. China
Keywords: New particle formation, Chloric acid, Particle formation
rate, Cluster concentration, Atmospheric nucleation precursor
*Corresponding authors. E-mail: shixl@sdnu.edu.cn

23 Abstract

24

25

26

27

28

29

30

31

32

33

34

35

36

37

38

39

40

41

Chlorine radicals are strong oxidizing agents in the atmosphere, and the process of chlorine oxidation results in the formation of chloric acid (HClO₃, CA). Recent studies have shown that trace amounts of CA have been detected in the Arctic boundary layer. However, the contribution of chlorine-containing species to oceanic new particle formation (NPF) has not been fully revealed. It is speculated that CA is involved in the oceanic nucleation process. In this study, the enhancement of CA-based NPF by dimethylamine (DMA) and sulfuric acid (SA) was comparatively investigated at the molecular level using density-functional theory (DFT) and atmospheric cluster dynamics simulation (ACDC). The results show that DMA can form clusters with CA through hydrogen bonding, halogen bonding and proton transfer, which reduces the energy barrier for CA-based cluster formation and significantly improves the thermodynamic stability of CA clusters. The cluster formation rate of CA-DMA cluster system is higher than that of the CA-SA cluster system. CA-DMA nucleation may not effectively contribute to Arctic NPF. These findings may help to reveal some of the missing sources of the Arctic NPF. The present study contributes to a deeper understanding of the influence of oceanic chlorine-containing constituents on the oceanic NPF.

42

1 Introduction

45

46

47

48

49

50

51

52

53

54

55

56

57

58

59

60

61

62

63

64

65

44

by regulating the radiative balance and climate of clouds(Moore et al., 2024; Revell et al., 2025). New particle formation (NPF) contributes to more than half of the global cloud condensation nuclei, which in turn contributes to cloud formation (Gordon et al., 2017; Takegawa et al., 2020; Williamson et al., 2019; Zhang et al., 2012; Zhao et al., 2024). Compared with clouds over land, ocean clouds cover a wider area and significantly increase the albedo of the ocean, so ocean clouds contribute more to the climate system (Merikanto et al., 2009; Wood, 2012; Zheng et al., 2021). Sulfuric acid (SA, H₂SO₄), methane sulfonic acid (MSA, CH₃HSO₃), and iodic acid (IA, HIO₃) are generally considered to contribute to the formation of oceanic particles (Hodshire et al., 2019; Yin et al., 2021; Facchini et al., 2008; Perraud et al., 2015; Arquero et al., 2017; Hopkins et al., 2008). However, there is still a significant difference between the particle formation rates observed in the field and those predicted by simulation (Kirkby et al., 2011; Kirkby et al., 2016; Zhang et al., 2004; Ehn et al., 2014; Dawson et al., 2012). Therefore, it is necessary to consider whether other gaseous precursors are involved in NPF to narrow the gap between experiments and simulations. Compared to the main atmospheric oxidants, hydroxyl radicals, chlorine radicals act as strong oxidants in the polar troposphere at relatively high concentration levels (Stone et al., 2012). The active chlorine cycle in the Arctic boundary layer during the spring after polar sunrise depletes O₃ in the region (Custard et al., 2016; Foster et al.,

Marine aerosols as the main natural aerosol system have a major global impact

2001; Thompson et al., 2015). Chloric acid (CA) has no photoactivity, with concentrations estimated to range from 1×10^5 to 7×10^6 molecules cm⁻³ (Tham et al., 2023). Research by Tham et al. indicates that the CA and perchloric acid (PA) observed in the Arctic atmosphere are primarily generated through homogeneous reactions involving chlorine, involving photochemical processes involving HO_x and bromine chemistry(Tham et al., 2023). Fang et al.(Fang et al., 2024) employed quantum mechanical/molecular mechanical methods to investigate that CA or PA may form as the final oxidation step of chlorine oxides. CA was not found in the particle phase of the aerosol, thus it is difficult to determine whether CA is involved in the NPF phase. Many studies have shown that atmospheric bases such as methylamine (MA), dimethylamine (DMA), trimethylamine (TMA) and ammonia can effectively enhance SA-based NPF (Yao et al., 2018; Almeida et al., 2013). Although amines emit 10–20 times less than ammonia in the ocean, amines can effectively form clusters with substances such as SA in the ocean (Myriokefalitakis et al., 2010; Semeniuk and Dastoor, 2018; Almeida et al., 2013). Of these amines, DMA has been found as a component of marine secondary aerosols (Facchini et al., 2008). Widely dispersed DMA has an atmospheric concentration of 0.4 - 10 pptv over the ocean and plays a key role in marine NPF(Van Pinxteren et al., 2019). DMA has been identified as the strongest enhancing atmospheric amine for SA and IA-driven NPF (Olenius et al., 2017; Ning et al., 2022). Thus, DMA may have a higher enhancing potential (EP) than

66

67

68

69

70

71

72

73

74

75

76

77

78

79

80

81

82

83

84

85

86

87

NH₃ for CA-based NPF.

Sulfuric acid (H₂SO₄, SA) has been detected in both gas and particulate phases in polluted coastal areas of China(Zhu et al., 2019; Yu et al., 2019). It is noteworthy that the concentration of SA is two orders of magnitude higher (up to 10⁸ molecules cm⁻³) in the coastal polluted areas due to urban air pollution compared to the clean marine atmosphere (Zhu et al., 2019). Sulfuric acid is poor nucleating agent in the atmosphere and promotes nucleation processes when combined with bases(Sipilä et al., 2010; Faloona, 2009). This precisely demonstrates the value of studying the CA-DMA system — it may serve as an additional source of acidic substances in the marine atmosphere. The nucleation of iodine species (oxyacids and oxides) is a current hot topic(Li et al., 2024; Ning et al., 2024). Additionally, extensive quantum chemical studies have been conducted on the clustering phenomena of sulfuric acid, methanesulfonic acid, and alkali compounds(Wu et al., 2023; Zhang et al., 2023). Engsvang et al. (Engsvang et al., 2024) has investigated the formation mechanism of CA clusters, concluding that CA did not contribute. The study by Engsvang was on fairly small clusters (up to 2 acid-base pairs). The formation rate and mechanism of larger CA-DMA clusters deserve further investigation. Using density functional theory (DFT) and the Atmospheric Clusters Dynamic Code (ACDC), the involvement of DMA and SA in the initial phase of CA-based NPF has been investigated. We obtained the minimum free energy structures of the $(CA)_{1-4}(DMA)_{1-4}$ and $(CA)_{1-4}(SA)_{1-4}$ clusters. The temperatures used in this study are within the temperature range of the atmospheric boundary layer in the ordinary

88

89

90

91

92

93

94

95

96

97

98

99

100

101

102

103

104

105

106

107

108

109

range(Miřijovský and Langhammer, 2015). The specific temperature value studied is

238, 258 and 278K. The concentration of CA was estimated to be in the range of $1.0 \times 10^6 - 1.0 \times 10^8$ molecules cm⁻³ based on measured data. The concentration of CA used is higher than the measured value and is intended solely for testing/prediction purposes. Further study of CA-DMA clusters under Arctic atmospheric conditions and the corresponding thermodynamic data used as input to the ACDC reveals the growth pathways and formation rates of the clusters.

116

117

118

119

120

121

122

123

124

125

126

127

128

129

130

131

115

110

111

112

113

114

2 Computational methods

Configurational Sampling

We employed a multi-step global minimum sampling scheme to search for the global minimum of (CA)₁₋₄(DMA)₁₋₄ and (CA)₁₋₄(SA)₁₋₄ clusters(Temelso et al., 2018; Schmitz and Elm, 2020). In this study, the initial structures of 1000-10000 (CA)₁₋₄(DMA)₁₋₄ and (CA)₁₋₄(SA)₁₋₄ clusters were randomly generated using the ABCluster software to determine their global minima (clusters with the lowest Gibbs free energies)(Odbadrakh et al., 2020; Zhang et al., 2018; Kubecka et al., 2019). In the multistep sampling scheme, the geometry optimization is performed at the PM7, $\omega B97X-D/6-31+G(d,p)$ and $\omega B97X-D/6-31++G(d,p)$ levels of theory, and the single-point energy calculations performed are at the DLPNO-CCSD(T)/aug-cc-pVTZ level of theory(Elm and Mikkelsen, 2014; Myllys et al., 2016). Geometry calculations are based on the ωB97X-D/6-31++G(d,p) theory level(Elm et al., 2020; Smith et al., 2021; Li et al., 2024; Ning et al., 2024; Wu et al., 2023). The GAUSSIAN 09 program package(Frisch et al., 2016) was used to perform

the PM7 and ω B97X-D calculations. DLPNO-CCSD(T) calculations were performed in the ORCA 4.0.0 program(Neese, 2012). For convergence problems and failures such as ending with a false frequency in the optimization of $(CA)_{1-4}(DMA)_{1-4}$ and $(CA)_{1-4}(SA)_{1-4}$ cluster geometries, the initial structures will be modified and re-optimized until the optimization is successful. The free energy of formation (ΔG) of individual clusters is calculated at different temperatures 238, 258, and 278 K. The structures of $(SA)_{1-4}$ and $(DMA)_{1-4}$ clusters were obtained from previous studies and are recalculated here(Xie et al., 2017).

Atmospheric Cluster Dynamics Code (ACDC) Simulation

Cluster formation rates, steady-state concentrations, and growth paths for $(CA)_{1-4}(DMA)_{1-4}$ and $(CA)_{1-4}(SA)_{1-4}$ clusters were calculated using ACDC without considering the effects of charge and water(Mcgrath et al., 2012). ACDC simulation conclusions are obtained based on the birth and death equation (Almeida et al., 2013; Lu et al., 2020; Kürten et al., 2018). The $(CA)_5(DMA)_5$ clusters are set as boundary clusters (see Supporting Information (SI) for details). The concentration ranges of [CA], [SA] and [DMA] were set to $10^6 - 10^8$ cm⁻³, $10^6 - 10^8$ cm⁻³ and 0.1 - 100 ppt, respectively. Widely dispersed DMA has an atmospheric concentration of 0.4 - 10 ppt over the ocean and plays a key role in marine NPF(Van Pinxteren et al., 2019). DMA at concentrations up to 100 ppt is primarily used for prediction.

3 Results and discussion

3.1 Cluster Structures and Cluster Formation Free Energy

To evaluate the thermodynamic stability of the formed CA-DMA clusters, the 154 formation free energies (ΔG , kcal mol⁻¹) at 278 K are calculated for the 155 156 $(CA)_{1-4}(DMA)_{1-4}$ clusters the at DLPNO-CCSD(T)/aug-cc-pVTZ//\omegaB97X-D/6-31++G(d,p) level of theory. As shown 157 158 in Figure. 1, hydrogen bonds play an important role in the formation of CA-DMA clusters. Proton transfer reactions are not observed in the pure (CA)₂ and (CA)₃ 159 clusters, whereas spontaneous proton transfer reactions are observed in all 160 $(CA)_{1-4}(DMA)_{1-4}$ clusters. For most $(CA)_{1-4}(DMA)_{1-4}$ clusters, protons are 161 transferred from CA to DMA. Proton transferring wasn't observed in pure (CA)2 and 162 (CA)₃ clusters, whereas spontaneous proton transfer reactions were present in all 163 $(CA)_{1-4}(DMA)_{1-4}$ clusters. For most $(CA)_{1-4}(DMA)_{1-4}$ clusters, protons are transferred 164 165 from CA to DMA, forming Cl-O...H-N hydrogen bonding, accompanied by the production of ClO₃⁻ negative ions and DMA⁺ ions. In CA-DMA clusters containing 166 two or more chlorine atoms, including (CA)₂(DMA)₁, (CA)₃(DMA)₁, (CA)₃(DMA)₁, 167 (CA)₃(DMA)₁, (CA)₃(DMA)₄, (CA)₄(DMA)₁, (CA)₄(DMA)₂, (CA)₄(DMA)₃, and 168 (CA)₄(DMA)₄ clusters, O-Cl...O-Cl halogen bonds and Cl-O...H-N hydrogen bonds 169 170 together stabilize these clusters described above. Halogen bonds are not present in clusters containing single Cl atom and in (CA)₂(DMA)₂, (CA)₂(DMA)₃, 171 (CA)₂(DMA)₄, as well as (CA)₃(DMA)₃ clusters. For the CA-SA clusters, the ClO₃⁻ 172 negative ions generated in the CA-DMA cluster system were not found in the CA-SA 173 cluster system because proton transfer do not occur. In contrast to the O-Cl...O-Cl 174 halogen bond found in the CA-DMA cluster system, the CA-SA cluster adds 175

S-O...Cl-O halogen bond (in the Figure S2). It is worth noting that the most stable cluster structure of CA-DMA we obtained exhibits similarities to the findings of Engsvang et al(Engsvang et al., 2024). CA-DMA clusters are primarily stabilized by hydrogen bonds.

The formation Gibbs free energy values of (A) (CA)₁₋₄(DMA)₁₋₄ and (B) (CA)₁₋₄(SA)₁₋₄ at 278 K and 1 atm are shown in Figure. 2. The Gibbs free energy values for the formation of (CA)₂, (CA)₃, and (CA)₄ clusters in the pure acid system are 1.31, 2.52, and 5.37 kcal mol⁻¹, respectively, implying that at 278 K, pure CA clusters are thermodynamically difficult to form. The difference between the ΔG values of (CA)₄(DMA)₄ cluster and (CA)₄(SA)₄ cluster is the largest, up to 61.62 kcal mol⁻¹. (CA)₁(SA)₁ and (CA)₁(DMA)₁ are both very important in their respective cluster systems, and their ΔG values are -2.62 and -10.08 kcal mol⁻¹, respectively⁻¹. The ΔG values of (CA)₁₋₄ clusters are 10.08 - 28.16 kcal mol⁻¹ higher than those of the corresponding (CA)₁₋₄(DMA)₁ clusters, suggesting that DMA stabilizes the CA clusters. As the size of CA-DMA clusters increases, the clusters gradually form a cage-symmetric structure. The ΔG values of the majority of clusters in the CA-DMA system are 3.55 - 61.62 kcal mol⁻¹ lower than the corresponding ΔG values of the CA-SA system. This indicates that the CA-DMA cluster system is more thermally stable compared to the CA-SA cluster system.

195

196

197

176

177

178

179

180

181

182

183

184

185

186

187

188

189

190

191

192

193

194

3.2 Evaporation Rates and Cluster Stability

The total evaporation rate $(\sum y, s^{-1})$ of $(CA)_{1-4}(DMA)_{1-4}$ clusters and

 $(CA)_{1-4}(SA)_{1-4}$ clusters formed at T = 278 K is shown in Figure. 3. The smaller value of $\sum y$ means that the stability of CA-DMA clusters is higher and the clusters shrink further. The clusters with the same number of CA molecules and the number of DMA molecules include (CA)₁(DMA)₁, (CA)₂(DMA)₂, (CA)₃(DMA)₃, and (CA)₄(DMA)₄ clusters, which have the values of $\Sigma \gamma$ of 10^2 , 2×10^{-4} , 5×10^{-1} , and 3×10^1 s⁻¹, respectively. $(CA)_2(DMA)_2$ cluster has the lowest $\sum \gamma$ value, implying that (CA)₂(DMA)₂ cluster is the most stable cluster in the "4 × 4" box system of CA-DMA clusters. For clusters with different numbers of CA and DMA molecules, the $\sum y$ value of (CA)₂(DMA)₁ cluster is significantly lower than that of other clusters, which indicates that (CA)₂(DMA)₁ cluster has a high probability of competing for the growth path of nucleation. In this study, we compare the evaporation rates of clusters from the CA-DMA system with those from the CA-SA system at 278K. In contrast to the other clusters, the evaporation rate of (CA)₁(SA)₄ clusters is lower than that of the corresponding (CA)₁(DMA)₄ clusters. The evaporation rates of most (CA)₁₋₄(DMA)₁₋₄ clusters are much smaller than those of the corresponding (CA)₁₋₄(SA)₁₋₄ clusters, indicating that the CA-DMA cluster system is kinetically more stable than the CA-SA cluster system.

215

216

217

218

219

198

199

200

201

202

203

204

205

206

207

208

209

210

211

212

213

214

3.3 Cluster Formation Rates and Steady-State Cluster Concentrations

Cluster formation rate (J) and steady-state CA dimer concentration ($\sum[(CA)_2]$) are important indicators for assessing the enhancement potential of DMA for CA-based nucleation. Figure 4 shows the variation of $\sum[(CA)_2]$ and J values at 278 K

with CA concentration ([CA] = $10^6 - 10^8$ cm⁻³) and DMA concentration ([DMA] = 1, 10 and 100 ppt). The J value of the CA-DMA system showed a positive correlation with CA and DMA concentrations as CA and DMA concentrations increased. The dependence of the cluster formation rate on the DMA concentration does not decrease with increasing CA concentration, which means that the dependence of the system on DMA does not saturate when the CA concentration is high. The $\sum [(CA)_2]$ and J of the CA-DMA system with the full range of acid-base concentrations considered (CA: 10⁶) - 10⁸ molecules cm⁻³, DMA: 1, 10 and 100 ppt) were significantly higher than the CA-SA system (Figure. S4). However, at high concentrations of [CA] = 1×10^7 molecules cm⁻³ and [DMA] = 10 ppt, the J value of the CA-DMA cluster system only reaches 1.39×10^{-11} cm⁻³ s⁻¹. The contribution of the CA-DMA cluster system to the NPF is not significant under the atmospheric conditions of 278 K. In addition, the CA-PA cluster system has a lower J value (Figure. S13-17). This may be due to the weak bond energies of Cl-O...Cl-O halogen bonds in the process of CA-PA nucleation (Figure. S12). Comparative studies indicate that the cluster formation rate of SA-DMA clusters exceeds that of CA-DMA clusters by more than seven orders of magnitude (Zhang et al., 2022). Under temperature and concentration parameters relevant to Arctic environments, the CA-DMA system could be incapable of forming cluster structures. Despite the negative outcome, this represents a significant advancement in advancing research on nucleation mechanisms in marine and Arctic regions.

220

221

222

223

224

225

226

227

228

229

230

231

232

233

234

235

236

237

238

239

240

241

To further systematically explore the effect of temperature on the J of the

CA-DMA cluster system, Figure. 5 shows the simulated J at other temperatures (238 and 258 K), [CA] = $10^6 - 10^8$ molecules cm⁻³, [DMA] = 0.1 ppt (red line), 1 ppt (green line), 10 ppt (blue line), and 100 ppt (black line). A comparison of the simulations at 258 K (Figure. 5a) and 238 K (Figure. 5b) reveals that the decrease in temperature further increases the J value of the CA-DMA cluster system to a higher level. However, at a low temperature (258 K), the J values of the CA-DMA cluster system do not reach higher levels at high concentrations of [CA] = 1×10^7 molecules cm⁻³ and [DMA] = 10 ppt. The J values of the CA-DMA cluster system were further investigated under cold Arctic conditions (238 K). It was found that the J value of CA-DMA cluster system at 238 K atmospheric condition was significantly higher than that of CA-DMA cluster system at other higher temperature conditions, which was mainly due to the fact that the low temperature attenuates the evaporation of CA-DMA clusters.

3.4 Cluster growth pathway

Figure 6 shows the growth paths of CA-DMA and CA-SA clusters at 278 K, [CA] = 10⁶ cm⁻³, [DMA] = 1 ppt, and [SA] = 10⁶ cm⁻³. The first step in the growth of CA-DMA clusters is the collision of a CA molecule and a DMA molecule to form a (CA)₁(DMA)₁ cluster. There are two growth paths for (CA)₁(DMA)₁ clusters: a CA molecule collides and combines with a (CA)₁(DMA)₁ cluster to form a (CA)₂(DMA)₁ cluster, and a DMA molecule is subsequently added to form a (CA)₂(DMA)₂ cluster; a (CA)₁(DMA)₁ cluster combines with another (CA)₁(DMA)₁ cluster to form a

(CA)₂(DMA)₂ cluster. This growth pattern is mainly due to the high stability of (CA)₂(DMA)₁ clusters. After the (CA)₂(DMA)₂ clusters, the growth route of the CA-DMA cluster system extends along the direct binding to the (CA)₁(DMA)₁ clusters. For (CA)₃(DMA)₃ clusters, one route is the addition of acid and base, and the other route is the direct binding to (CA)₁(DMA)₁ clusters to produce (CA)₄(DMA)₄ clusters. Compared to the nucleation pathways observed at 278K in the CA-DMA system, pathways at 238K involve in the formation of (CA)₂(DMA)₂ to (CA)₂(DMA)₄ clusters, as well as the combination of (CA)₄(DMA)₄ clusters with a single (CA)₁(DMA)₁ cluster to generate (CA)₅(DMA)₅ clusters.

The growth pathway of the CA-SA cluster system differs considerably from that of the CA-DMA cluster system. The cluster initially formed in the CA-SA cluster system is the $(CA)_2$ cluster not the $(CA)_1(SA/DMA)_1$ cluster in the CA-DMA system. After the generation of $(CA)_2$ cluster, the system can generate $(CA)_3(SA)_1$ clusters by successive addition of acid molecules. Subsequently, $(CA)_3(SA)_1$ clusters combine with $(CA)_1(SA)_1$ clusters to generate $(CA)_3(SA)_2$ clusters. The final $(CA)_4(SA)_4$ cluster of the system is generated by collision of a $(CA)_3(SA)_2$ cluster with an $(SA)_2$ cluster.

3.5 Atmospheric implications and conclusions

In this paper, combination method of quantum chemistry and ACDC were used to elucidate the molecular structure mechanism of DMA and SA enhancing role of CA nucleation by comparing the CA-DMA and CA-SA nucleation systems. Proton

transfer was observed in all (CA)₁₋₄(DMA)₁₋₄ clusters while no proton transfer occurred within (CA)₁₋₄(SA)₁₋₄ clusters. The ClO₃⁻ groups generated by the deprotonation of CA are involved in the formation of at least one hydrogen bond. Hydrogen and halogen bonds together stabilize the CA-DMA and CA-SA nucleation systems. The vast majority of CA-SA cluster systems have higher ΔG values than the corresponding CA-DMA cluster systems. The cluster formation rates of the pure CA-PA and CA-SA nucleation systems are relatively low, and the contribution of DMA to CA nucleation is stronger than that of SA. Clusters with the same number of CA and DMA molecules ((CA)₁(DMA)₁, (CA)₂(DMA)₂, (CA)₃(DMA)₃, and (CA)₄(DMA)₄ clusters) play a key role in the growth path of CA-DMA clusters, which is consistent with the existing literature(Wu et al., 2023; Zhang et al., 2023). This study is important for a deeper understanding of Arctic atmospheric nucleation. The current simulations do not take into account charge effects, the involvement of water molecules, and the influence of complex atmospheric matrices (e.g., organic matter). In the future, it is necessary to validate the simulation results with field observations and extend it to multi-component (e.g., IA/SA/DMA mixing or CA-SA-DMA clusters) nucleation systems in order to quantify the contribution of chlorine-containing substances to the global NPF in a more comprehensive way.

304

305

307

286

287

288

289

290

291

292

293

294

295

296

297

298

299

300

301

302

303

Data availability

All data supported the paper are available from the article, supplementary information,

and the corresponding author upon reasonable request.

Acknowledgements The work was financially supported by National Natural Science Foundation of China (project No. 22276114). **Additional information Competing interests:** The authors declare no competing financial interests. **Author Contributions Statement Shengming Wang:** Investigation, Conceptualization, Formal analysis, Data curation, Writing-original draft. Huidi Zhang: Investigation. Xiangli Shi: Methodology, Writing-reviewing and editing, Validation, Supervision. Qingzhu Zhang: Methodology, Validation, Supervision, Funding acquisition. Wenxing Wang: Resources, Funding acquisition, Writing-reviewing and editing Supervision. Qiao Wang: Resources.

References

- Almeida, J., Schobesberger, S., Kürten, A., Ortega, I. K., Kupiainen-Määttä, O., Praplan, A. P., Adamov,
- A., Amorim, A., Bianchi, F., and Breitenlechner, M.: Molecular understanding of sulphuric acid-amine
- particle nucleation in the atmosphere, Nature, 502, 359-363, 2013.
- Arquero, K. D., Xu, J., Gerber, R. B., and Finlayson-Pitts, B. J.: Particle formation and growth from
- 336 oxalic acid, methanesulfonic acid, trimethylamine and water: a combined experimental and theoretical
- study, Physical Chemistry Chemical Physics, 19, 28286-28301, 2017.
- Custard, K. D., Pratt, K. A., Wang, S., and Shepson, P. B.: Constraints on Arctic atmospheric chlorine
- production through measurements and simulations of Cl2 and ClO, Environ. Sci. Technol., 50,
- 340 12394-12400, 2016.
- Dawson, M. L., Varner, M. E., Perraud, V., Ezell, M. J., Gerber, R. B., and Finlayson-Pitts, B. J.:
- 342 Simplified mechanism for new particle formation from methanesulfonic acid, amines, and water via
- experiments and ab initio calculations, Proceedings of the National Academy of Sciences, 109,
- 344 18719-18724, 2012.
- Ehn, M., Thornton, J. A., Kleist, E., Sipilä, M., Junninen, H., Pullinen, I., Springer, M., Rubach, F.,
- Tillmann, R., and Lee, B.: A large source of low-volatility secondary organic aerosol, Nature, 506,
- 347 476-479, 2014.
- Elm, J. and Mikkelsen, K. V.: Computational approaches for efficiently modelling of small atmospheric
- clusters, Chemical Physics Letters, 615, 26-29, 2014.
- 350 Elm, J., Kubečka, J., Besel, V., Jääskeläinen, M. J., Halonen, R., Kurten, T., and Vehkamäki, H.:
- 351 Modeling the formation and growth of atmospheric molecular clusters: A review, Journal of Aerosol
- 352 Science, 149, 105621, 2020.
- Engsvang, M., Knattrup, Y., Kubecka, J., and Elm, J.: Chlorine Oxyacids Potentially Contribute to
- 354 Arctic Aerosol Formation, Environmental Science & Technology Letters, 11, 101-105, 2024.
- Facchini, M. C., Decesari, S., Rinaldi, M., Carbone, C., Finessi, E., Mircea, M., Fuzzi, S., Moretti, F.,
- 356 Tagliavini, E., and Ceburnis, D.: Important source of marine secondary organic aerosol from biogenic
- amines, Environmental science & technology, 42, 9116-9121, 2008.
- 358 Faloona, I.: Sulfur processing in the marine atmospheric boundary layer: A review and critical
- assessment of modeling uncertainties, Atmospheric Environment, 43, 2841-2854, 2009.
- 360 Fang, Y.-G., Wei, L., Francisco, J. S., Zhu, C., and Fang, W.-H.: Mechanistic Insights into Chloric Acid
- 361 Production by Hydrolysis of Chlorine Trioxide at an Air-Water Interface, Journal of the American
- 362 Chemical Society, 146, 21052-21060, 2024.
- Foster, K. L., Plastridge, R. A., Bottenheim, J. W., Shepson, P. B., Finlayson-Pitts, B. J., and Spicer, C.
- 364 W.: The role of Br2 and BrCl in surface ozone destruction at polar sunrise, Science, 291, 471-474,
- 365 2001.
- Frisch, M., Trucks, G., Schlegel, H., Scuseria, G., Robb, M., Cheeseman, J., Scalmani, G., Barone, V.,
- Petersson, G., and Nakatsuji, H.: Gaussian 16, Revision A. 03, Gaussian, Inc., Wallingford CT, 3, 2016.
- Gordon, H., Kirkby, J., Baltensperger, U., Bianchi, F., Breitenlechner, M., Curtius, J., Dias, A.,
- Dommen, J., Donahue, N. M., and Dunne, E. M.: Causes and importance of new particle formation in
- the present day and preindustrial atmospheres, Journal of Geophysical Research: Atmospheres, 122,
- 371 8739-8760, 2017.

- Hodshire, A. L., Campuzano-Jost, P., Kodros, J. K., Croft, B., Nault, B. A., Schroder, J. C., Jimenez, J.
- L., and Pierce, J. R.: The potential role of methanesulfonic acid (MSA) in aerosol formation and
- growth and the associated radiative forcings, Atmospheric Chemistry and Physics, 19, 3137-3160,
- 375 2019.
- Hopkins, R. J., Desyaterik, Y., Tivanski, A. V., Zaveri, R. A., Berkowitz, C. M., Tyliszczak, T., Gilles,
- 377 M. K., and Laskin, A.: Chemical speciation of sulfur in marine cloud droplets and particles: Analysis of
- 378 individual particles from the marine boundary layer over the California current, Journal of Geophysical
- 379 Research: Atmospheres, 113, 2008.
- 380 Kirkby, J., Curtius, J., Almeida, J., Dunne, E., Duplissy, J., Ehrhart, S., Franchin, A., Gagné, S., Ickes,
- 381 L., and Kürten, A.: Role of sulphuric acid, ammonia and galactic cosmic rays in atmospheric aerosol
- 382 nucleation, Nature, 476, 429-433, 2011.
- Kirkby, J., Duplissy, J., Sengupta, K., Frege, C., Gordon, H., Williamson, C., Heinritzi, M., Simon, M.,
- Yan, C., and Almeida, J.: Ion-induced nucleation of pure biogenic particles, Nature, 533, 521-526,
- 385 2016.
- Kubecka, J., Besel, V., Kurten, T., Myllys, N., and Vehkamaki, H.: Configurational sampling of
- 387 noncovalent (atmospheric) molecular clusters: sulfuric acid and guanidine, The Journal of Physical
- 388 Chemistry A, 123, 6022-6033, 2019.
- Kürten, A., Li, C., Bianchi, F., Curtius, J., Dias, A., Donahue, N. M., Duplissy, J., Flagan, R. C., Hakala,
- 390 J., and Jokinen, T.: New particle formation in the sulfuric acid-dimethylamine-water system:
- 391 reevaluation of CLOUD chamber measurements and comparison to an aerosol nucleation and growth
- model, Atmospheric Chemistry and Physics, 18, 845-863, 2018.
- 393 Li, J., Ning, A., Liu, L., and Zhang, X.: Atmospheric Bases-Enhanced Iodic Acid Nucleation:
- 394 Altitude-Dependent Characteristics and Molecular Mechanisms, Environmental Science & Technology,
- 395 58, 16962-16973, 2024.
- 396 Lu, Y., Liu, L., Ning, A., Yang, G., Liu, Y., Kurtén, T., Vehkamäki, H., Zhang, X., and Wang, L.:
- 397 Atmospheric sulfuric acid dimethylamine nucleation enhanced by trifluoroacetic acid, Geophysical
- 398 Research Letters, 47, e2019GL085627, 2020.
- 399 McGrath, M., Olenius, T., Ortega, I., Loukonen, V., Paasonen, P., Kurtén, T., Kulmala, M., and
- 400 Vehkamäki, H.: Atmospheric Cluster Dynamics Code: a flexible method for solution of the birth-death
- 401 equations, Atmospheric Chemistry and Physics, 12, 2345-2355, 2012.
- 402 Merikanto, J., Spracklen, D., Mann, G., Pickering, S., and Carslaw, K.: Impact of nucleation on global
- 403 CCN, Atmospheric Chemistry and Physics, 9, 8601-8616, 2009.
- 404 Miřijovský, J. and Langhammer, J.: Multitemporal monitoring of the morphodynamics of a
- 405 mid-mountain stream using UAS photogrammetry, Remote sensing, 7, 8586-8609, 2015.
- 406 Moore, A. N., Cancelada, L., Ke'La A, K., and Prather, K. A.: Secondary aerosol formation from
- 407 mixtures of marine volatile organic compounds in a potential aerosol mass oxidative flow reactor,
- 408 Environmental Science: Atmospheres, 4, 351-361, 2024.
- 409 Myllys, N., Elm, J., and Kurten, T.: Density functional theory basis set convergence of sulfuric
- 410 acid-containing molecular clusters, Computational and Theoretical Chemistry, 1098, 1-12, 2016.
- 411 Myriokefalitakis, S., Vignati, E., Tsigaridis, K., Papadimas, C., Sciare, J., Mihalopoulos, N., Facchini,
- 412 M., Rinaldi, M., Dentener, F., and Ceburnis, D.: Global modeling of the oceanic source of organic
- 413 aerosols, Adv, Meteorol, 939171, 2010.
- Neese, F.: The ORCA program system, Wiley Interdisciplinary Reviews: Computational Molecular
- 415 Science, 2, 73-78, 2012.

- Ning, A., Liu, L., Zhang, S., Yu, F., Du, L., Ge, M., and Zhang, X.: The critical role of dimethylamine
- 417 in the rapid formation of iodic acid particles in marine areas, npj Climate and Atmospheric Science, 5,
- 418 92, 2022.
- Ning, A., Shen, J., Zhao, B., Wang, S., Cai, R., Jiang, J., Yan, C., Fu, X., Zhang, Y., and Li, J.:
- 420 Overlooked significance of iodic acid in new particle formation in the continental atmosphere,
- Proceedings of the National Academy of Sciences, 121, e2404595121, 2024.
- Odbadrakh, T. T., Gale, A. G., Ball, B. T., Temelso, B., and Shields, G. C.: Computation of atmospheric
- 423 concentrations of molecular clusters from ab initio thermochemistry, 2020.
- Olenius, T., Halonen, R., Kurtén, T., Henschel, H., Kupiainen Määttä, O., Ortega, I. K., Jen, C. N.,
- 425 Vehkamäki, H., and Riipinen, I.: New particle formation from sulfuric acid and amines: Comparison of
- 426 monomethylamine, dimethylamine, and trimethylamine, Journal of Geophysical Research:
- 427 Atmospheres, 122, 7103-7118, 2017.
- 428 Perraud, V., Horne, J. R., Martinez, A. S., Kalinowski, J., Meinardi, S., Dawson, M. L., Wingen, L. M.,
- Dabdub, D., Blake, D. R., and Gerber, R. B.: The future of airborne sulfur-containing particles in the
- absence of fossil fuel sulfur dioxide emissions, Proceedings of the National Academy of Sciences, 112,
- 431 13514-13519, 2015.
- Revell, L. E., Edkins, N. J., Venugopal, A. U., Bhatti, Y. A., Kozyniak, K. M., Davy, P. K., Kuschel, G.,
- 433 Somervell, E., Hardacre, C., and Coulson, G.: Marine aerosol in Aotearoa New Zealand: implications
- for air quality, climate change and public health, Journal of the Royal Society of New Zealand, 55,
- 435 1339-1361, 2025.
- 436 Schmitz, G. and Elm, J.: Assessment of the DLPNO binding energies of strongly noncovalent bonded
- atmospheric molecular clusters, ACS omega, 5, 7601-7612, 2020.
- 438 Semeniuk, K. and Dastoor, A.: Current state of aerosol nucleation parameterizations for air-quality and
- 439 climate modeling, Atmos. Environ., 179, 77-106, 2018.
- 440 Sipilä, M., Berndt, T., Petäjä, T., Brus, D., Vanhanen, J., Stratmann, F., Patokoski, J., Mauldin III, R. L.,
- 441 Hyvärinen, A.-P., and Lihavainen, H.: The role of sulfuric acid in atmospheric nucleation, Science, 327,
- 442 1243-1246, 2010.
- 443 Smith, J. N., Draper, D. C., Chee, S., Dam, M., Glicker, H., Myers, D., Thomas, A. E., Lawler, M. J.,
- and Myllys, N.: Atmospheric clusters to nanoparticles: Recent progress and challenges in closing the
- gap in chemical composition, Journal of Aerosol Science, 153, 105733, 2021.
- Stone, D., Whalley, L. K., and Heard, D. E.: Tropospheric OH and HO 2 radicals: field measurements
- and model comparisons, Chemical Society Reviews, 41, 6348-6404, 2012.
- Takegawa, N., Seto, T., Moteki, N., Koike, M., Oshima, N., Adachi, K., Kita, K., Takami, A., and
- Kondo, Y.: Enhanced new particle formation above the marine boundary layer over the Yellow Sea:
- 450 Potential impacts on cloud condensation nuclei, Journal of Geophysical Research: Atmospheres, 125,
- 451 e2019JD031448, 2020.
- 452 Temelso, B., Morrison, E. F., Speer, D. L., Cao, B. C., Appiah-Padi, N., Kim, G., and Shields, G. C.:
- 453 Effect of mixing ammonia and alkylamines on sulfate aerosol formation, The Journal of Physical
- 454 Chemistry A, 122, 1612-1622, 2018.
- Tham, Y. J., Sarnela, N., Iyer, S., Li, Q., Angot, H., Quéléver, L. L., Beck, I., Laurila, T., Beck, L. J.,
- 456 and Boyer, M.: Widespread detection of chlorine oxyacids in the Arctic atmosphere, Nature
- 457 Communications, 14, 1769, 2023.
- Thompson, C., Shepson, P., Liao, J., Huey, L., Apel, E., Cantrell, C., Flocke, F., Orlando, J., Fried, A.,
- and Hall, S.: Interactions of bromine, chlorine, and iodine photochemistry during ozone depletions in

- 460 Barrow, Alaska, Atmospheric Chemistry and Physics, 15, 9651-9679, 2015.
- 461 van Pinxteren, M., Fomba, K. W., van Pinxteren, D., Triesch, N., Hoffmann, E. H., Cree, C. H.,
- 462 Fitzsimons, M. F., von Tümpling, W., and Herrmann, H.: Aliphatic amines at the Cape Verde
- 463 Atmospheric Observatory: Abundance, origins and sea-air fluxes, Atmos. Environ., 203, 183-195,
- 464 2019.
- Williamson, C. J., Kupc, A., Axisa, D., Bilsback, K. R., Bui, T., Campuzano-Jost, P., Dollner, M., Froyd,
- 466 K. D., Hodshire, A. L., and Jimenez, J. L.: A large source of cloud condensation nuclei from new
- particle formation in the tropics, Nature, 574, 399-403, 2019.
- Wood, R.: Stratocumulus clouds, Monthly weather review, 140, 2373-2423, 2012.
- 469 Wu, N., Ning, A., Liu, L., Zu, H., Liang, D., and Zhang, X.: Methanesulfonic acid and iodous acid
- 470 nucleation: a novel mechanism for marine aerosols, Physical Chemistry Chemical Physics, 25,
- 471 16745-16752, 2023.
- Xie, H.-B., Elm, J., Halonen, R., Myllys, N., Kurten, T., Kulmala, M., and Vehkamaki, H.: Atmospheric
- fate of monoethanolamine: enhancing new particle formation of sulfuric acid as an important removal
- process, Environmental science & technology, 51, 8422-8431, 2017.
- 475 Yao, L., Garmash, O., Bianchi, F., Zheng, J., Yan, C., Kontkanen, J., Junninen, H., Mazon, S. B., Ehn,
- 476 M., and Paasonen, P.: Atmospheric new particle formation from sulfuric acid and amines in a Chinese
- 477 megacity, Science, 361, 278-281, 2018.
- 478 Yin, R., Yan, C., Cai, R., Li, X., Shen, J., Lu, Y., Schobesberger, S., Fu, Y., Deng, C., and Wang, L.:
- 479 Acid-base clusters during atmospheric new particle formation in urban Beijing, Environmental Science
- 480 & Technology, 55, 10994-11005, 2021.
- Yu, H., Ren, L., Huang, X., Xie, M., He, J., and Xiao, H.: Iodine speciation and size distribution in
- 482 ambient aerosols at a coastal new particle formation hotspot in China, Atmospheric Chemistry and
- 483 Physics, 19, 4025-4039, 2019.
- Zhang, H., Li, H., Liu, L., Zhang, Y., Zhang, X., and Li, Z.: The potential role of malonic acid in the
- 485 atmospheric sulfuric acid-ammonia clusters formation, Chemosphere, 203, 26-33, 2018.
- Zhang, R., Khalizov, A., Wang, L., Hu, M., and Xu, W.: Nucleation and growth of nanoparticles in the
- 487 atmosphere, Chemical reviews, 112, 1957-2011, 2012.
- 488 Zhang, R., Ma, F., Zhang, Y., Chen, J., Elm, J., He, X.-C., and Xie, H.-B.: HIO3-HIO2-Driven
- 489 Three-Component Nucleation: Screening Model and Cluster Formation Mechanism, Environmental
- 490 Science & Technology, 58, 649-659, 2023.
- 491 Zhang, R., Suh, I., Zhao, J., Zhang, D., Fortner, E. C., Tie, X., Molina, L. T., and Molina, M. J.:
- 492 Atmospheric new particle formation enhanced by organic acids, Science, 304, 1487-1490, 2004.
- 493 Zhang, R., Xie, H.-B., Ma, F., Chen, J., Iyer, S., Simon, M., Heinritzi, M., Shen, J., Tham, Y. J., and
- 494 Kurten, T.: Critical role of iodous acid in neutral iodine oxoacid nucleation, Environmental Science &
- 495 Technology, 56, 14166-14177, 2022.
- Zhao, B., Donahue, N. M., Zhang, K., Mao, L., Shrivastava, M., Ma, P.-L., Shen, J., Wang, S., Sun, J.,
- 497 and Gordon, H.: Global variability in atmospheric new particle formation mechanisms, Nature, 631,
- 498 98-105, 2024.
- Zheng, G., Wang, Y., Wood, R., Jensen, M. P., Kuang, C., McCoy, I. L., Matthews, A., Mei, F.,
- 500 Tomlinson, J. M., and Shilling, J. E.: New particle formation in the remote marine boundary layer,
- Nature communications, 12, 527, 2021.
- Zhu, Y., Li, K., Shen, Y., Gao, Y., Liu, X., Yu, Y., Gao, H., and Yao, X.: New particle formation in the
- 503 marine atmosphere during seven cruise campaigns, Atmospheric Chemistry and Physics, 19, 89-113,

504 2019.

Graphical Abstract

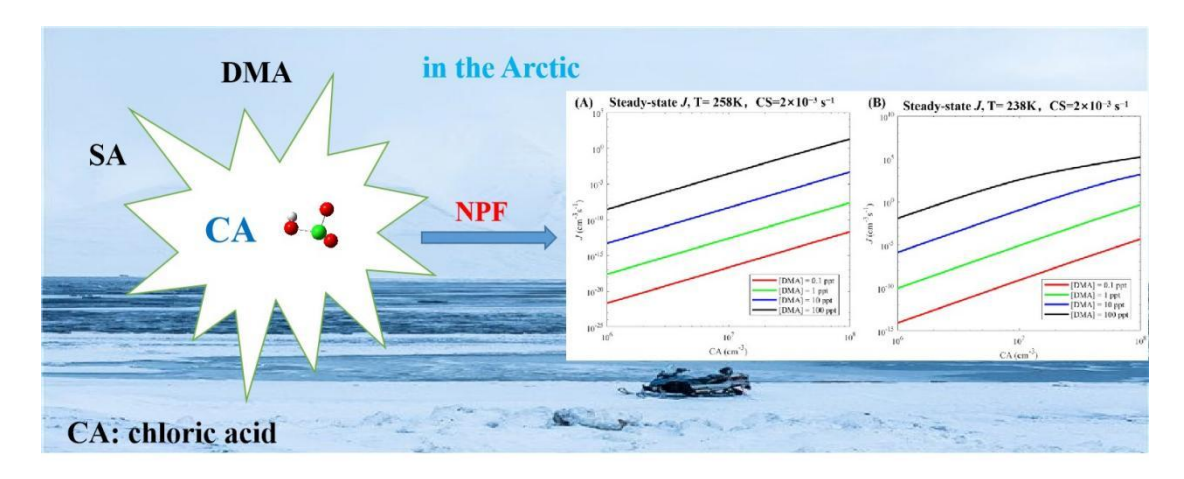


Figure Captions

- Figure 1. Identified lowest free energy structures of the (CA)₁₋₄(DMA)₁₋₄ clusters at
- the DLPNO-CCSD(T)/aug-cc-pVTZ// ω B97X-D/6-31++G(d,p) level of theory. The
- red, blue, gray, green and white balls represent oxygen, nitrogen, carbon, chlorine and
- 535 hydrogen atoms, respectively. The dashed white and black lines indicate hydrogen
- and halogen bonds, respectively.

- Figure 2. The formation free energy (ΔG) (in kcal mol⁻¹) of (A) (CA)₁₋₄(DMA)₁₋₄ and
- 538 (B) $(CA)_{1-4}(SA)_{1-4}$ clusters at the
- 539 DLPNO-CCSD(T)/aug-cc-pVTZ// ω B97X-D/6-31++G(d,p) level of theory. The
- calculations are performed at 278 K and 1 atm.
- Figure 3. Evaporation rates for (A) $(CA)_{1-4}(DMA)_{1-4}$ and (B) $(CA)_{1-4}(SA)_{1-4}$ clusters
- clusters at 278 K and 1 am.
- Figure 4. Simulated steady-state CA dimer concentration $\sum [(CA)_2]$ (cm⁻³) (A) and
- the cluster formation rates J (cm⁻³ s⁻¹) out of the simulation systems (B) as a function
- 545 of [CA] at 278 K.
- Figure 5. The simulated cluster formation rate J (cm⁻³ s⁻¹) of the CA-DMA system at
- different temperatures (A) 258, and (B) 238 K; $[CA] = 10^6 10^8$ molec. cm⁻³; [DMA]
- 548 = 0.1, 1, 10, and 100 ppt; and $CS = 2 \times 10^{-3} \text{ s}^{-1}$.
- Figure 6. (A) Main clustering pathways of (CA)₁₋₄(DMA)₁₋₄ clusters at 278 K, [CA]
- $= 10^6 \text{ cm}^{-3}$, and [DMA] = 5 ppt. (B) Main clustering pathways of $(CA)_{1-4}(SA)_{1-4}$
- clusters at 278 K, $[CA] = 10^6 \text{ cm}^{-3}$, and $[SA] = 10^6 \text{ cm}^{-3}$. (C) Main clustering
- pathways of $(CA)_{1-4}(DMA)_{1-4}$ clusters at 238 K, $[CA] = 10^6$ cm⁻³, and [DMA] = 5

553 ppt.

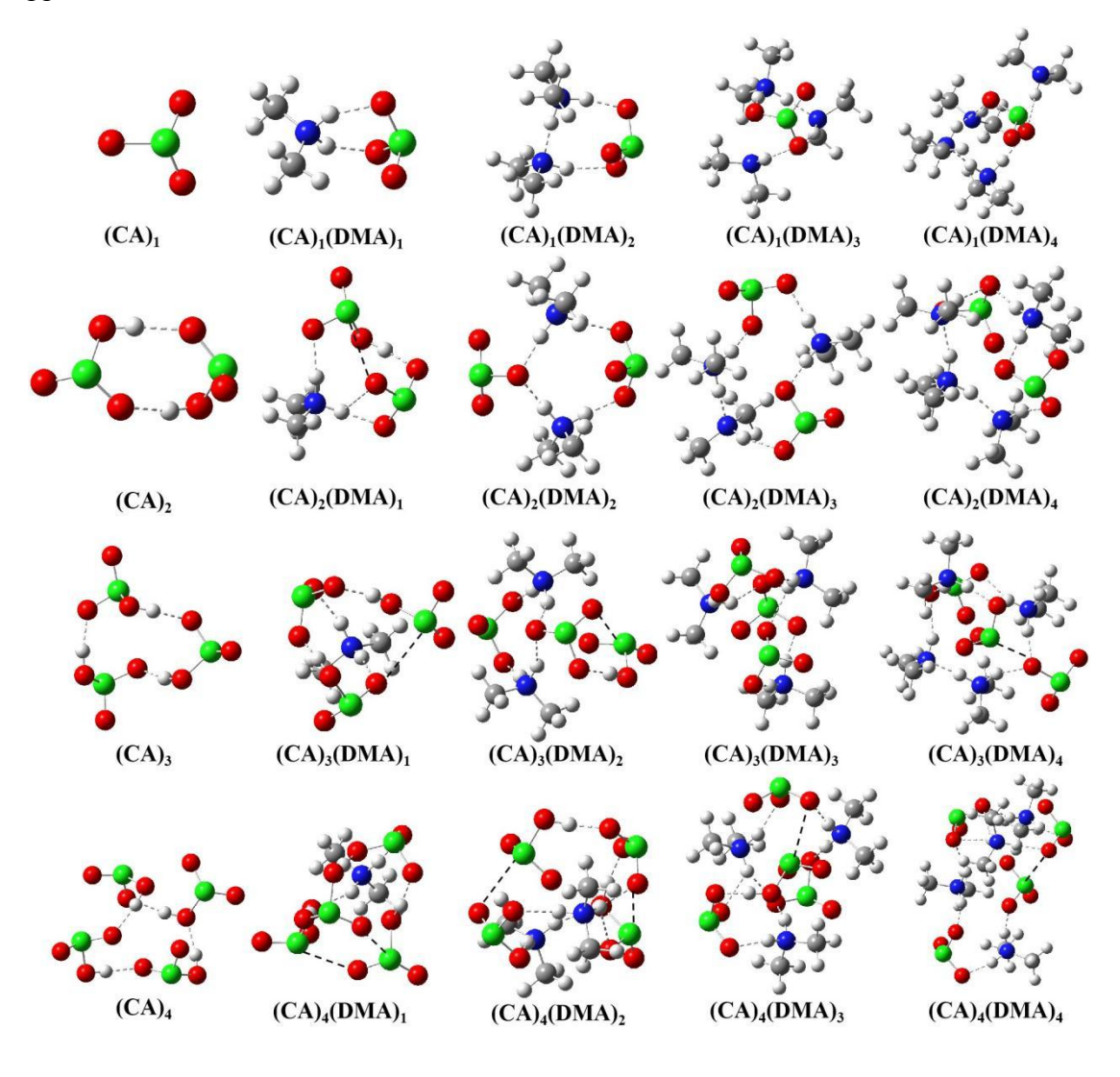


Figure 1. Identified lowest free energy structures of the $(CA)_{1-4}(DMA)_{1-4}$ clusters at the DLPNO-CCSD(T)/aug-cc-pVTZ// ω B97X-D/6-31++G(d,p) level of theory. The red, blue, gray, green and white balls represent oxygen, nitrogen, carbon, chlorine and hydrogen atoms, respectively. The dashed white and black lines indicate hydrogen and halogen bonds, respectively.

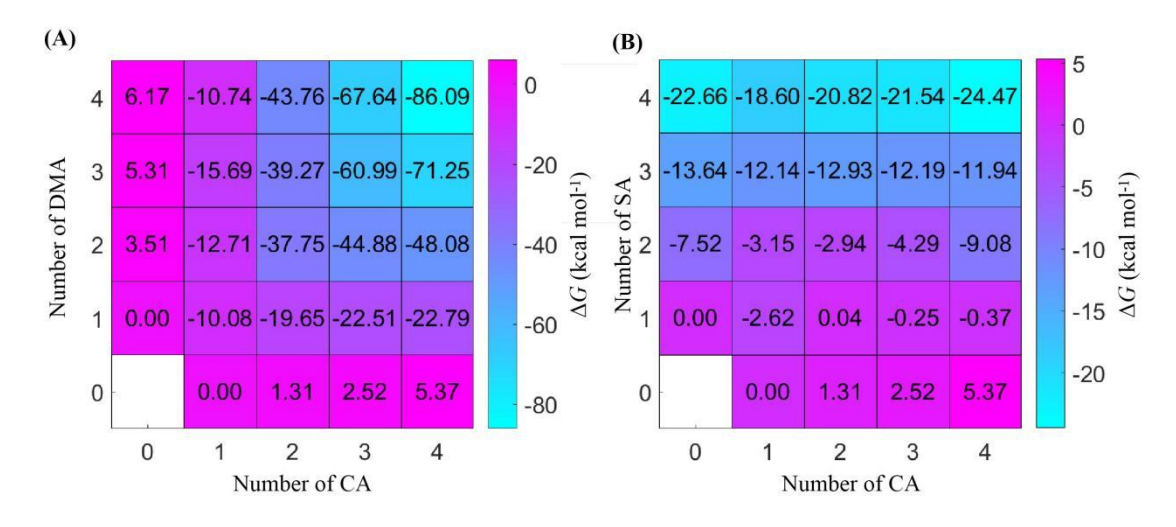


Figure 2. The formation free energy (ΔG) (in kcal mol⁻¹) of (A) (CA)₁₋₄(DMA)₁₋₄ and

(B) $(CA)_{1-4}(SA)_{1-4}$ clusters at the

DLPNO-CCSD(T)/aug-cc-pVTZ//ωB97X-D/6-31++G(d,p) level of theory. The

calculations are performed at 278 K and 1 atm.

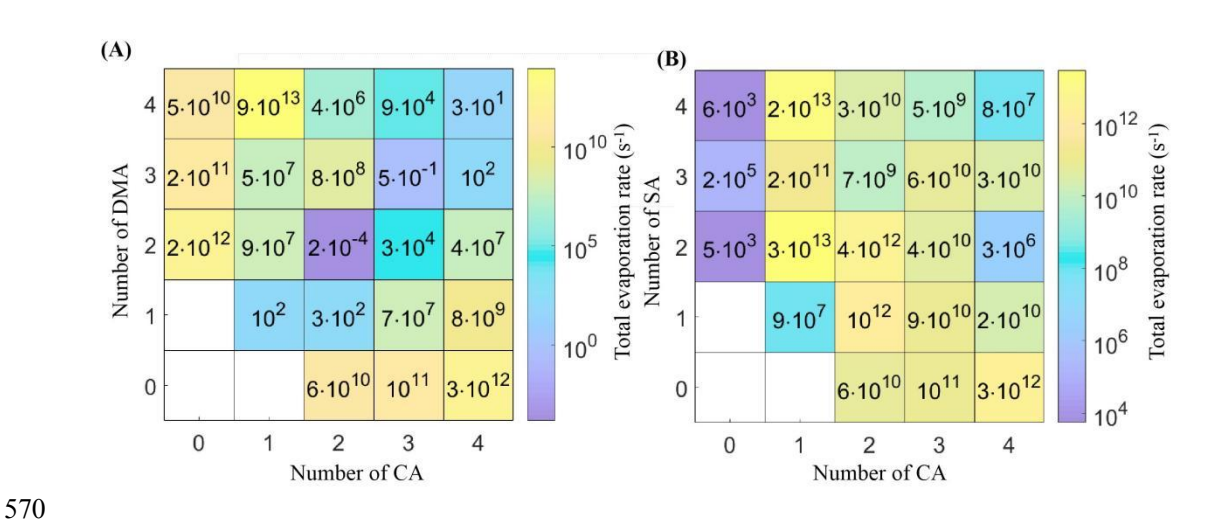


Figure 3. Evaporation rates for (A) $(CA)_{1-4}(DMA)_{1-4}$ and (B) $(CA)_{1-4}(SA)_{1-4}$ clusters clusters at 278 K and 1 am.

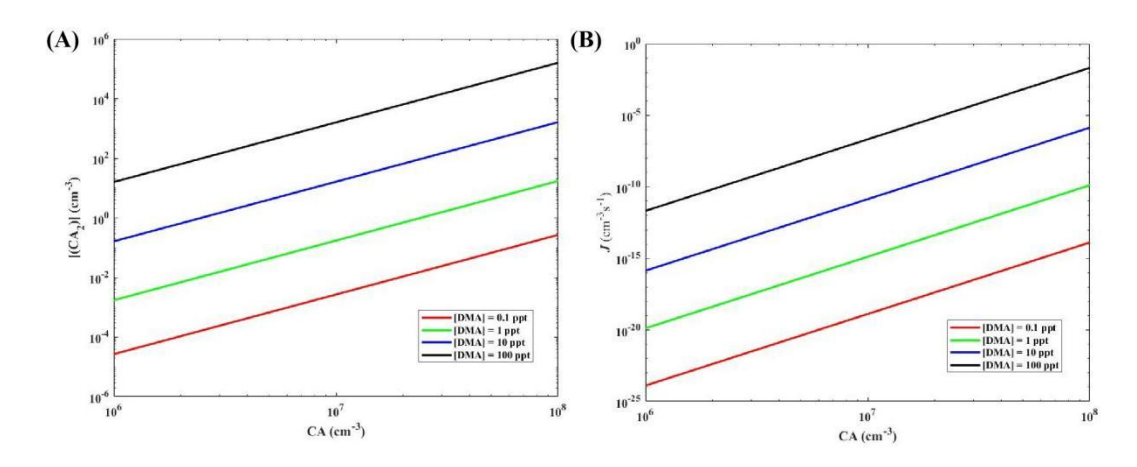


Figure 4. Simulated steady-state CA dimer concentration $\sum [(CA)_2]$ (cm⁻³) (A) and the cluster formation rates J (cm⁻³ s⁻¹) out of the simulation systems (B) as a function of [CA] at 278 K.

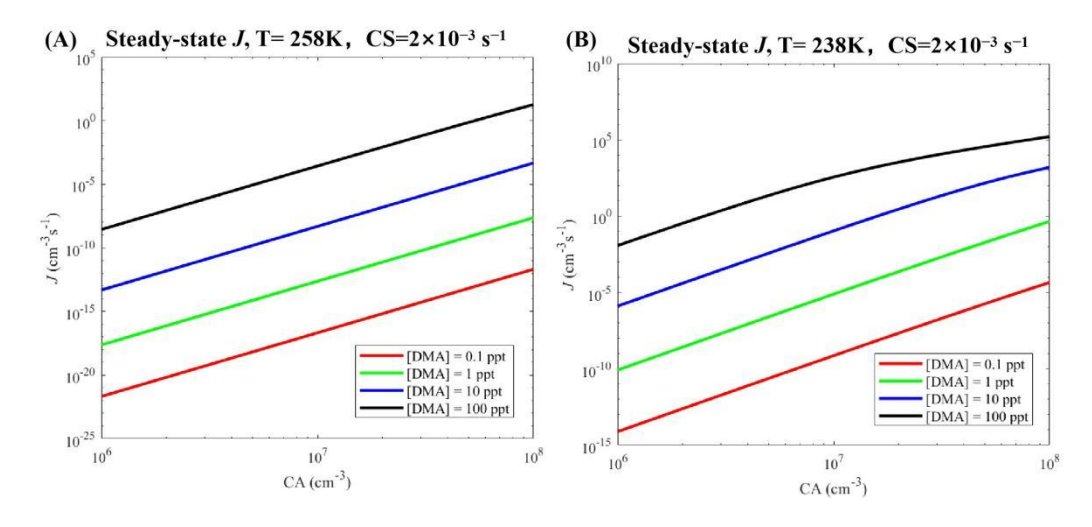


Figure 5. The simulated cluster formation rate J (cm⁻³ s⁻¹) of the CA-DMA system at different temperatures (A) 258, and (B) 238 K; [CA] = $10^6 - 10^8$ molec. cm⁻³; [DMA] = 0.1, 1, 10, and 100 ppt; and CS = 2×10^{-3} s⁻¹.

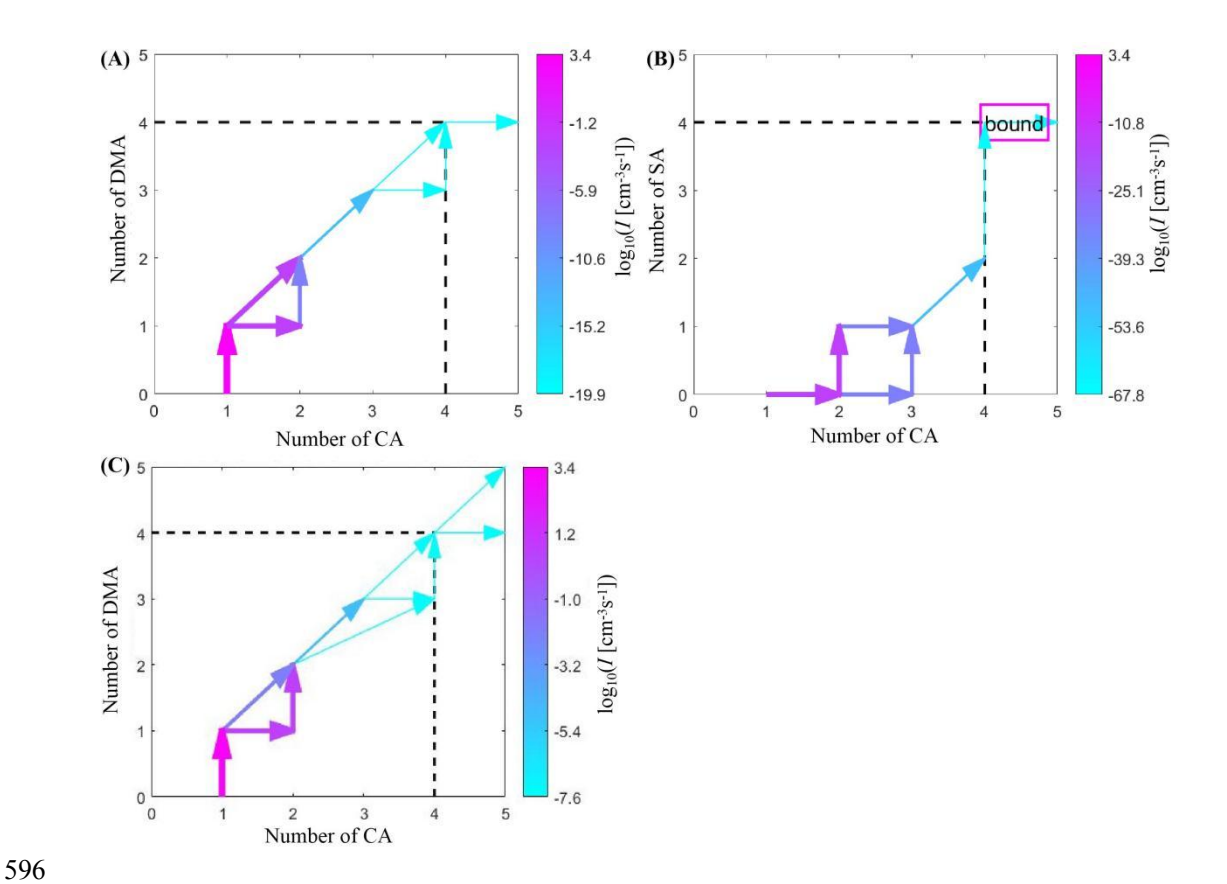


Figure 6. (A) Main clustering pathways of $(CA)_{1-4}(DMA)_{1-4}$ clusters at 278 K, [CA] = 10^6 cm⁻³, and [DMA] = 5 ppt. (B) Main clustering pathways of $(CA)_{1-4}(SA)_{1-4}$ clusters at 278 K, [CA] = 10^6 cm⁻³, and [SA] = 10^6 cm⁻³. (C) Main clustering pathways of $(CA)_{1-4}(DMA)_{1-4}$ clusters at 238 K, [CA] = 10^6 cm⁻³, and [DMA] = 5 ppt.